ENABLING CONTINUOUS PILOT-SCALE WET SPINNING OF CHITIN MULTIFILAMENT YARNS: SPINNERET EFFECTS AND SOLVENT REMOVAL CONTROL

Irina Kuznik[1,a,*,#], Carolin König[1,b,*,#], Enrico Sommer[1,c], Sabrina Scheele[1,d], Lukas Benecke[1,e], Chokri Cherif[1,f]

[1] – Institute of Textile Machinery and High Performance Material Technology (ITM), TUD Dresden University of Technology, Hohe Str. 6, 01069 Dresden, Germany
[a] – ORCID: 0000-0002-2291-153X, [b] – ORCID: 0009-0008-3757-5867,
[c] – ORCID: 0009-0000-3871-2917, [d] – ORCID: 0009-0002-1265-3060,
[e] – ORCID: 0000-0002-3198-5610, [f] – ORCID: 0000-0001-8077-6922
**corresponding authors: irina.kuznik@tu-dresden.de, carolin.koenig@tu-dresden.de*
[#]Irina Kuznik and Carolin König are considered joint first authors, as they contributed equally to this work

Abstract

Chitin-based filament yarns have great potential for use in biomedical and technical textiles. However, their processing and applicability are severely limited by poor solubility and inefficient solvent removal, restricting scalable manufacturing. This study investigates the development and scale-up of a wet spinning process for chitin yarns using the ionic liquid 1-ethyl-3-methylimidazolium propionate (EMIMOPr). Solvent removal during monofilament spinning was investigated using Fourier-transform infrared spectroscopy and thermogravimetric analysis to examine its dependence on filament diameter, coagulation temperature, and residence time. The results demonstrated that solvent removal is governed by mass transport processes, with residual solvent potentially persisting in the filament core under laboratory-scale conditions. Based on these insights, multifilament spinning on a pilot scale was successfully implemented, enabling efficient solvent removal during coagulation and washing stages. The resulting yarns exhibited homogeneous morphology and consistent textile-mechanical properties. This process provides a promising platform for the large-scale production of chitin filament yarns for advanced biomedical and technical applications.

Keywords: *chitin, multifilament yarns, wet spinning, ionic liquids, solvent removal*

Received: 20.01.2026
Accepted: 22.04.2026

1. Introduction

Fibre-based structures are particularly well suited to regenerative medicine and tissue engineering applications, as they can be manufactured to withstand different loads, offer a high surface-to-volume ratio, and closely mimic the natural fibre structures of the human body (e.g. collagen and elastin fibres) [1]. This results in a large specific surface area, tunable porosity and pore interconnectivity, all of which promote cell adhesion, proliferation and efficient nutrient transport [2]. In this context, biocompatible and resorbable biopolymers, such as chitin and its derivatives, are a promising class of biomaterials. Chitin exhibits all the key properties required for biomedical applications, including controlled biodegradability, low immunogenicity and high mechanical strength, which arises from its pronounced crystallinity [3]. Compared with chitosan, which is generally more amorphous and mechanically less robust due to its higher degree of deacetylation (DD), chitin offers superior structural stability and strength retention, which is particularly advantageous for load-bearing fibrous implants and textile-based reinforcements. These characteristics make chitin a promising candidate for soft tissue implants, such as hernia meshes, tendon substitutes, and surgical sutures [3, 4]. Beyond soft-tissue applications, chitin has attracted considerable interest in regenerative medicine for its beneficial effects on bone defect healing [5–8]. Combined with other properties, such as antibacterial and odour-inhibiting effects and high mechanical strength, chitin holds great potential for various applications in the textile industry. Furthermore, chitin is a sustainable, biodegradable biopolymer that is widely available, with an estimated 10^{11}–10^{14} tons constantly present in the biosphere [9]. However, existing studies predominantly focus on films, nanofibres, fibre blends or hydrogels rather than continuous filament yarns [10–14].

Despite its favourable properties, the processing of chitin remains challenging due to its semi-crystalline structure and highly stable intermolecular hydrogen bonding network, which severely limit its solubility. Chitin is insoluble in common solvents such as water, organic solvents and mildly acidic or alkaline solutions, which significantly restricts the scalability of manufacturing processes. However, chitin has been shown to be soluble in various solvent systems, including dimethylacetamide (DMAc)/LiCl mixtures, $CaBr_2 \cdot H_2O$-saturated methanol, hexafluoroisopropanol, hexafluoroacetone, lithium thiocyanate, phosphoric acid and N-methyl-2-pyrrolidone (NMP) [15]. Pure chitin fibre spinning largely relies on solvent mixtures such as trichloroacetic acid/methylene chloride [16], formic acid/dichloroacetic acid [17, 18] or DMAc/LiCl [19, 20]. Although these solvent systems can dissolve chitin, many are toxic, corrosive, poorly biodegradable, or mutagenic [21]. Consequently, research and material development have predominantly focused on chitosan rather than chitin itself [4, 8]. Furthermore, the incomplete removal of conventional solvents from spun filament yarns poses a major challenge, especially for medical applications, which are subject to strict regulatory requirements. Additionally, acidic solutions are unsuitable for drug delivery systems, as many bioactive compounds, such as enzymes, peptides, and proteins, are highly sensitive to acidic environments, thereby limiting functionalisation strategies [22, 23]. These constraints highlight the urgent need for novel, highly efficient, and safe solvent systems and processing routes for chitin filament yarns to fully exploit the material's potential.

Recent approaches that use more environmentally friendly, sustainable ionic liquids (ILs) as solvents have demonstrated considerable progress in developing a continuous spinning process for chitosan- and chitin-based fibres [24, 25]. Despite increasing interest in IL-based processing of chitin, the mechanisms governing solvent removal during fibre formation remain poorly understood, particularly under conditions relevant for continuous

filament spinning. While existing studies largely focus on solubility and material properties, the interplay between filament geometry, coagulation conditions, and solvent removal kinetics has not yet been systematically investigated [24, 26–28]. Furthermore, most investigations are confined to laboratory-scale systems, and the transfer of these findings to continuous multifilament spinning processes remains unclear. In this context, a detailed understanding of solvent removal mechanisms is essential, as incomplete removal can critically affect fibre structure, mechanical performance, and application potential.

The aim of this study is therefore to investigate solvent removal during IL-based wet spinning of chitin and to translate these findings into a robust, scalable multifilament spinning process. The focus is on identifying critical process parameters influencing solvent removal, filament formation, and yarn properties, thereby providing a process-oriented framework for the scalable production of solvent-free chitin multifilament yarns.

2. Materials and Methods

2.1. Materials

Chitin from Arctic shrimps (*Pandalus borealis*) with a DD of 3.62% and a molecular weight (M_W) of 540 kDa, in the following referred to as CH-SHR, was purchased from Chitinor AS (Tromsø, Norway). The IL 1-ethyl-3-methylimidazolium propionate (purity ≥95%), in the following referred to as EMIMOPr, was supplied by proionic GmbH (Raaba-Grambach, Austria). The water content of the IL was determined by Karl-Fisher titration (TitroLine® 7500, SI Analytics, Mainz, Germany) and was found to be 0.414%.

2.2. Preparation of Chitin/Ionic Liquid Spinning Dopes

Chitin spinning dopes with a total volume of 3 L were prepared using a high-shear dissolver (DISPERMAT® CN20 F2, VMA-Getzmann GmbH, Reichshof, Germany). To obtain defined polymer concentrations of 4 and 5 wt.% (120 g and 150 g of chitin, respectively), chitin powder and EMIMOPr were added sequentially. The mixture was then homogenised at 90 °C and 650 rpm for 2 h, and the progress of chitin dissolution was investigated using light microscopy (Imager.M1 with an AxioCam MRc5 digital camera, Carl Zeiss, Oberkochen, Germany). For this purpose, dope samples (~3 mL) were collected from the mixture at defined time intervals (0, 30, 60, 90, and 120 min) and analysed for the presence of undissolved particles. The prepared spinning dopes were then transferred to the spinning tank of the wet-spinning plant (Fourné Maschinenbau GmbH, Alfter-Impekoven, Germany) and degassed at 60 °C for 24 h prior to spinning.

2.3. Rheological Characterisation of Spinning Dopes

The rheological behaviour and temperature-dependent flow properties of the prepared chitin spinning dopes were investigated using a cone-plate rheometer (HAAKE MARS II, Thermo Fisher Scientific Inc., Waltham, MA, USA) equipped with a titanium cone (35 mm diameter, 2° angle). A constant gap of 0.100 mm was used for all measurements. To evaluate the temperature-dependent rheological behaviour of EMIMOPr/CH-SHR spinning dopes, oscillatory shear measurements were performed over a frequency range of 1–100 Hz and a temperature range of 25–100 °C, relevant for the spinning process. The complex viscosity $|\eta^*|$ [Pa·s] was determined using the Cox-Merz relationship [29] and was used as an indicator of the flow behaviour under processing conditions. Data analysis was performed using HAAKE RheoWin software (Thermo Fisher Scientific Inc., Waltham, MA, USA) and Origin 2019 (OriginLab Corporation, Northampton, MA, USA).

2.4. Investigation of Solvent Removal during Chitin Monofilament Spinning

To investigate the solvent removal behaviour of IL during fibre formation, chitin/EMIMOPr spinning dopes were extruded into a temperature-controlled coagulation bath filled with deionised water using a high-pressure syringe pump (Fusion 6000, Chemyx Inc., Stafford, TX, USA) and curved dosing cannulas (Gonano Dosiertechnik GmbH, Breitstetten, Austria) as spinnerets (Figure 1). A continuous filament take-up system (slow-winder, DIENES Apparatebau GmbH, Mühlheim am Main, Germany) was used. The influence of the following key process parameters was systematically investigated: coagulation bath temperature (T_C), fibre residence time in the coagulation bath (t_C) and dosing cannula diameter (d_S). T_C values of 70, 80, and 90 °C were applied, as well as t_C of 1, 2, 5, 15, and 30 min. Additionally, d_S values of 0.6, 0.69, and 0.84 mm were investigated. The coagulation bath had a length of 80 cm, corresponding to a t_C of approximately 2 min under continuous spinning conditions at a take-up speed of 0.4 m/min. Different t_C values were achieved by either adjusting the distance between the extrusion unit and the winder or by using discontinuous batch spinning with defined immersion times.

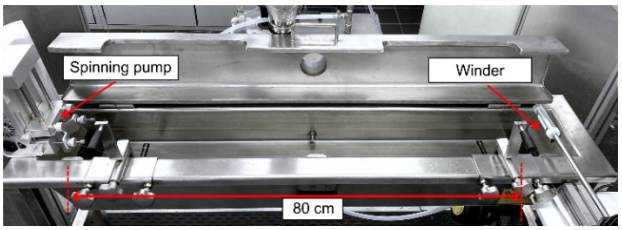

Figure 1. Experimental setup of a spinning process for continuous spinning of chitin monofilaments on a laboratory scale.

2.5. Spinning of Chitin Multifilament Yarns

Chitin multifilament yarn spinning was carried out using a pilot-scale solvent wet spinning line (Fourné Maschinenbau GmbH, Alfter-Impekoven, Germany). For the spinning process, the degassed spinning dope (5 wt.%) was heated to 80 °C and extruded through a spinneret assembly into a coagulation bath (CB) containing deionised water. The resulting chitin multifilament yarns were then washed in three consecutive washing baths (WB) containing deionised water (WB1, WB2) and ethanol (WB3), dried in a godet drying unit, and wound onto spools.

Three different spinneret geometries were employed for the spinning trials: 148 capillaries with a diameter of 70 µm (70 µm/148f), 300 capillaries with a diameter of 90 µm (90 µm/300f) and 24 capillaries with a diameter of 160 µm (160 µm/24f). The selected geometries allowed the filament diameter and total filament count to be varied systematically, thereby enabling the influence of these factors on filament formation, solvent removal and process stability to be investigated. The overall drawing ratio of the multifilament yarns was adjusted by altering the rotational speeds of the six godet units arranged sequentially along the spinning line. The aim was to identify an optimal balance between maximum draw and stable filament formation, while avoiding filament breakage. Particular attention was given to avoiding excessive stress concentrations that could cause filament rupture at the spinneret or between the godet units. The spinning dope was delivered by a gear pump (1.2 cm^3/rev) operating at speeds between 6 and 25 rpm. Depending on the spinneret geometry, the pump speed was adjusted to optimise the volumetric flow rate and ensure stable filament extrusion. A comprehensive overview

of the applied process parameters, including delivery rates, spinneret geometries, final drawing ratios and take-up speeds, is provided in Table 1. The overall drawing ratio is defined as the ratio of the take-up speed to the volumetric extrusion rate at the spinneret and may therefore take values below unity under the applied processing conditions. The corresponding thermal conditions along the spinning line, including the temperatures of the spinning dope, CB, WB1–WB3, and the drying stage, are summarised in Table 2.

Table 1. Process parameters applied for the multifilament spinning of EMIMOPr/CH-SHR spinning dopes.

Yarn sample	Delivery volume [cm^3/min]	Delivery rate [m/min]	Capillary diameter [µm]	Nozzle holes [n]	Drawing ratio	Take-up speed [m/min]
CH-SHR-1	18	31.60	70	148	0.29	9.2
CH-SHR-2	24	12.58	90	300	0.83	10.5
CH-SHR-3	24	12.58	90	300	0.95	12.0
CH-SHR-4	7.2	14.92	160	24	0.64	9.6

Table 2. Process temperatures applied for the multifilament spinning of EMIMOPr/CH-SHR-based spinning dopes.

Yarn sample	Temperature [°C]					
	spinning dope	coagulation bath	washing bath 1	washing bath 2	washing bath 3	drying unit
CH-SHR-1	80	73	85	88	22	80
CH-SHR-2	80	71	86	88	22	80
CH-SHR-3	80	69	86	89	22	80
CH-SHR-4	80	70	87	89	22	80

2.6. Morphological Examination

Scanning electron microscopy (SEM) was used to analyse the surface morphology of the fibres using an ESEM QUANTA FEG 250 microscope (FEI Company, Hillsboro, OR, USA), operated at an accelerating voltage of 3.5 kV and a magnification of 2000×.

For cross-sectional analysis, fibre samples were embedded in epoxy resin and then ground and polished. The prepared cross-sections were then examined using a light microscope (Imager.M1 with an AxioCam MRc5 digital camera, Carl Zeiss, Oberkochen, Germany). Image acquisition and analysis were performed using ZEN software (Carl Zeiss, Oberkochen, Germany).

2.7. Infrared Spectroscopy (FTIR)

Fourier-transform infrared (FTIR) spectroscopy was used to analyse the chemical structure of the chitin filaments and the raw material. Spectra were recorded using the attenuated total reflection (ATR) technique on a Nicolet 6700 FTIR spectrometer (Thermo Fisher Scientific, Waltham, MA, USA). For each measurement, 64 scans were averaged over a wavenumber range of 4000–600 cm^{-1} at a spectral resolution of 4 cm^{-1}. Spectral evaluation was performed using OMNIC™ Spectra software (Thermo Fisher Scientific, Waltham, MA, USA). To investigate solvent removal along the spinning line, fibre samples (~10 cm) were collected at defined positions during the spinning process: immediately after the CB and after each washing stage (WB1-WB3). After sampling,

the multifilament yarns were dried in a desiccator for 24 h to remove any residual moisture or coagulation medium. These samples were then formed into compact bundles with a diameter of ~10 mm and analysed by FTIR spectroscopy, as described above.

2.8. Thermogravimetric Analysis (TGA)

Thermogravimetric analysis (TGA) was conducted using a Q500 thermogravimetric analyser and TA Universal Analysis software (TA Instruments, New Castle, DE, USA). Fibre sampling and conditioning were performed in the same manner as for the FTIR measurements. After drying in a desiccator for 24 h, the multifilament yarns were cut into short fibre segments (~1–2 mm). Measurements were performed over the temperature range of 30–800 °C at a heating rate of 40 K/min under a nitrogen purge atmosphere. For each measurement, 10–15 mg of sample was placed in a pre-tared ceramic crucible. High-resolution (*HiRes*) mode was applied to enable accurate discrimination of individual thermal degradation stages.

2.9. Textile-Physical Characterisation

The linear density of the chitin fibres was determined gravimetrically in accordance with DIN EN ISO 1973. The average linear density was calculated according to equation (1):

$$\overline{\varrho}_{l,b} = \frac{m_b}{\sum_{i=1}^{100} l_i} \cdot 10^4 \quad (1)$$

where:

$\overline{\varrho}_{l,b}$ – mean linear density [dtex];

m_b – weight of the filament bundle [mg];

l_i – length of the i fibres in the bundle [mm].

Tensile and elongation properties were determined in accordance with DIN EN ISO 5079 using a ZwickLine Z2.5 tensile testing machine and testXpert III software (ZwickRoell, Ulm, Germany) under standard climate conditions (20 °C, 65% relative humidity). Specimens were tested at a gauge length of 250 mm and a crosshead speed of 250 mm/min. A preload force of 0.05 N was applied, and a 100 N load cell was used for all measurements.

3. Results and Discussion

3.1 Preparation and Characterisation of Spinning Dopes

Figure 2 shows the results of the light microscopy investigation into the thermally assisted dissolution process of chitin spinning dopes (CH-SHR), with polymer concentrations of 4 and 5 wt.%, in EMIMOPr, as a function of dissolution time. Immediately after preparation, all samples exhibited a similar appearance, characterised by large, swollen chitin aggregates, indicating the initial penetration of the IL into the polymer structure. As the treatment time increased, progressive dissolution was observed. After 60 min, the samples appeared almost completely dissolved, with only minor residual heterogeneities detectable. Following prolonged treatment, only a few undissolved particles remained, confirming the process's high dissolution efficiency. No significant differences in dissolution behaviour were observed between the two polymer concentrations investigated, indicating that both 4 and 5 wt.% solutions can be processed under comparable conditions.

The high dissolution capability of EMIMOPr for chitin is consistent with the literature [30, 31], which attributes this behaviour to the propionate anion's ability to effectively

disrupt intermolecular hydrogen bonding within the polysaccharide network. Consequently, homogeneous spinning dopes with chitin concentrations of up to 5 wt.% can be produced under relatively mild processing conditions (≤ 90 °C, ≤ 2 h). This demonstrates the suitability of EMIMOPr as a process-compatible solvent, highlighting its potential of this system for scalable fibre spinning processes.

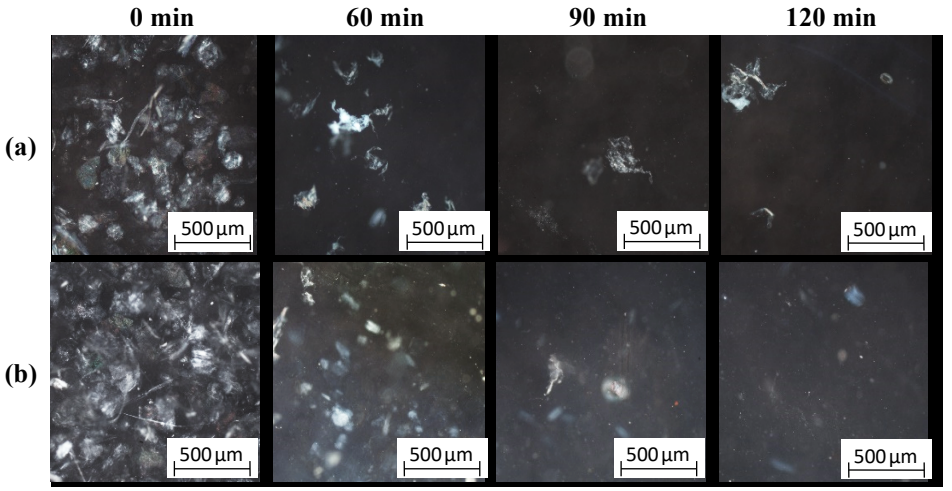

Figure 2. Light microscopic analysis of the dissolution behaviour of EMIMOPr/CH-SHR spinning dopes at different treatment times (0, 60, 90, and 120 min) and chitin concentrations: (a) 4 wt.%, (b) 5 wt.%.

Rheological investigations of the EMIMOPr/CH-SHR spinning dopes revealed a pronounced dependence of the complex viscosity |η*| on both temperature and polymer concentration. Figure 3 shows the temperature-dependent viscosity profiles of spinning dopes containing 4 wt.% and 5 wt.% of chitin. For both solutions, viscosity decreased continuously with increasing temperature over the investigated range of 25–100 °C. This behaviour is characteristic of thermally activated polymer solutions and can be attributed to increased molecular mobility and reduced intermolecular interactions at elevated temperatures [32, 33]. Additionally, the polymer concentration was clearly found to influence the viscosity. The 5 wt.% solution exhibited significantly higher viscosities across the entire temperature range compared to the 4 wt.% solution. For instance, at 70 °C, the viscosity of the 5 wt.% solution (85.0 Pa·s) was considerably higher than that of the 4 wt.% solution (16.8 Pa·s, Figure 3). This increase in viscosity with rising polymer content can be explained by stronger intermolecular interactions and reduced chain mobility, resulting from the number of dissolved polymer chains in the system [32, 33].

These rheological characteristics directly impact the spinnability of the solutions. Based on empirical processing limits, viscosities in the range of approximately 50–100 Pa·s are considered suitable for stable filament formation in wet spinning processes [25, 34]. The investigated solutions therefore exhibit favourable viscosities within a temperature range of approximately 70–80 °C, ensuring both sufficient flowability and adequate chain entanglement for filament formation. Consequently, this temperature range was selected as the operating window for subsequent spinning experiments, providing a balance between process stability and fibre formation quality.

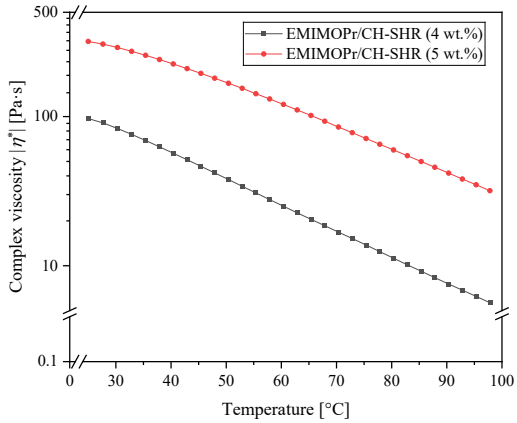

Figure 3. Temperature-dependent complex viscosity |η*| of EMIMOPr/CH-SHR spinning dopes at different chitin concentrations (4 wt.% and 5 wt.%).

3.2. Investigation of Solvent Removal During Chitin Monofilament Spinning

3.2.1. Infrared Spectroscopy (FTIR)

The FTIR spectra of the solvent EMIMOPr and CH-SHR are shown in Figure 4. The characteristic absorption bands of EMIMOPr reported in the literature were clearly identified at 2965 cm^{-1} (C–H stretching), 1560 cm^{-1} (C=N stretching), 1380 cm^{-1} (C–H bending) and 1175 cm^{-1} (C=O stretching) (Figure 4A) [35, 36]. The FTIR spectrum of CH-SHR exhibited the typical vibrational regions of N–H, O–H and C–H stretching at 3400–3480 cm^{-1} and 2877 cm^{-1}, the amide I and amide II bands at 1623–1660 cm^{-1} and 1556 cm^{-1} (C=O stretching and N–H bending, respectively), the amide III band at 1315 cm^{-1} (C–N stretching) and C–O–C stretching vibrations at 1100–1000 cm^{-1} (Figure 4B) [37, 38]. The pronounced C=N absorption band of EMIMOPr at 1560 cm^{-1} was therefore selected as a reliable marker for detecting residual solvent within the spun chitin monofilaments.

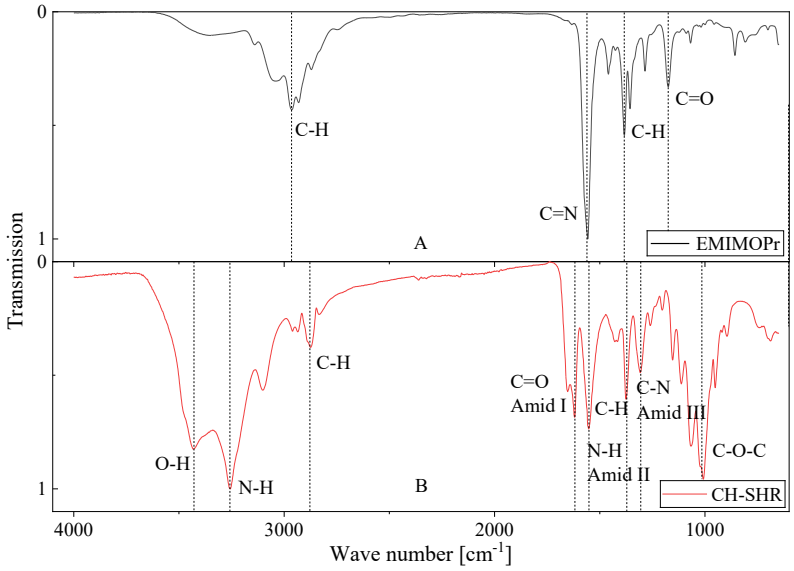

Figure 4. FTIR spectra of (A) EMIMOPr and (B) CH-SHR.

Figure 5 shows the FTIR spectra of the manufactured chitin monofilaments. Based on the preliminary spectral analysis, the wavenumber range of 1425–1700 cm^{-1}, encompassing the amide I and amide II bands of chitin, as well as the C=N band of EMIMOPr, was used to assess the solvent removal behaviour of the chitin monofilaments. Reference spectra of EMIMOPr (grey) and CH-SHR (red) are included for comparison.

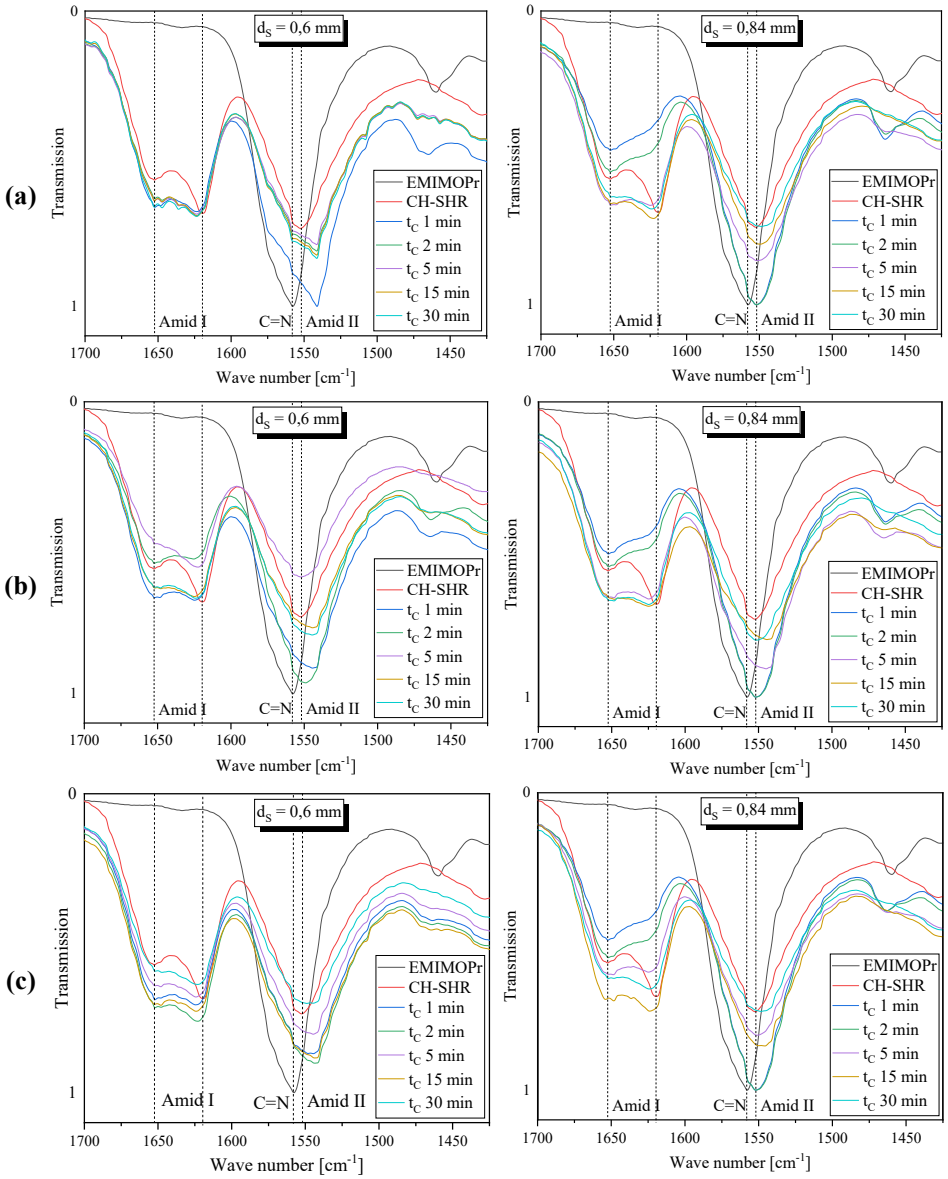

Figure 5. Comparison of FTIR spectra in the range of 1425–1700 cm^{-1} of EMIMOPr, CH-SHR and chitin monofilaments, varying coagulation time (t_C) and spinneret diameter (d_S) at coagulation bath temperatures (T_C) of (a) 70 °C, (b) 80 °C, and (c) 90 °C.

Figure 6 shows the FTIR spectra of chitin monofilaments obtained at T_C of 80 °C and 90 °C, with t_C of 5 and 2 min, respectively, for different d_S. Pronounced differences in residual solvent content were observed depending on filament diameter.

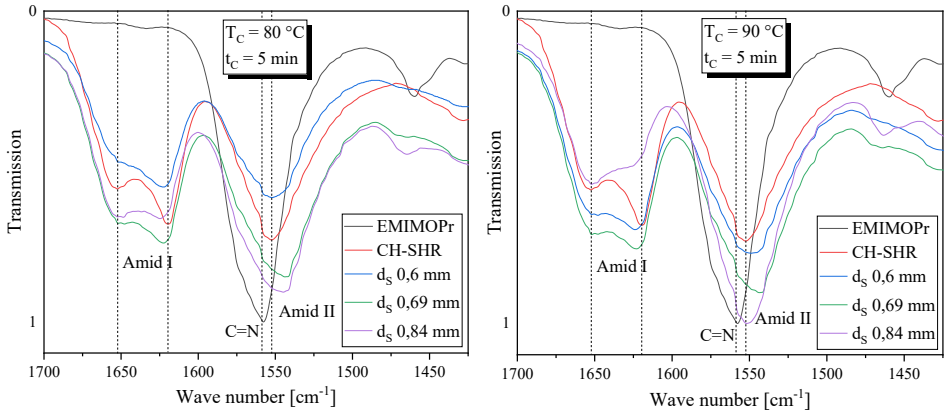

Figure 6. Comparison of FTIR spectra in the range of 1425–1700 cm^{-1} of EMIMOPr, CH-SHR and chitin monofilaments spun with spinneret diameters (d_S) of 0.6, 0.69, and 0.84 mm at coagulation conditions of (a) 5 min and 80 °C, and (b) 2 min and 90 °C.

At a T_C of 70 °C, EMIMOPr remained detectable in all spun chitin monofilaments, regardless of the d_S. In both experimental series, complete solvent removal could only be achieved after t_C of ≥ 30 min (Figure 5a). However, monofilaments spun with a smaller diameter (d_S = 0.6 mm) already exhibited substantially reduced EMIMOPr content after 2 min compared to filaments spun with a larger diameter (d_S = 0.84 mm). At a T_C of 80 °C, complete solvent removal was achieved in 15 min for thicker filaments (d_S = 0.84 mm) and in just 5 min for thinner filaments (d_S = 0.6 mm) (Figure 5b). Further increasing T_C to 90 °C resulted in no or only marginally detectable EMIMOPr residues after residence times of 5 min (d_S = 0.84 mm) and 2 min (d_S = 0.6 mm), respectively (Figure 5c).

These results clearly demonstrate that reducing the filament diameter significantly accelerates solvent removal during coagulation, indicating shortened transport pathways within the filament [39]. Accordingly, pronounced differences in residual solvent content were observed as a function of d_S. Filaments spun with d_S of 0.84 mm and 0.69 mm still exhibited considerable EMIMOPr residues after 5 min in the coagulation bath at 80 °C (Figure 6a), whereas only negligible or no solvent traces were detected at a d_S of 0.6 mm. Increasing T_C to 90 °C reduced the residence time required for solvent removal to 2 min (Figure 6b). However, the non-uniform distribution of the solvent and coagulation medium concentrations across the filament cross-section suggests that the detection limit of FTIR spectroscopy is constrained by the infrared beam's shallow penetration depth (~0.5–3 µm) [40]. Consequently, FTIR analysis primarily reflects solvent removal at or near the filament surface. Therefore, to assess residual solvent content within the filament core, complementary TGA measurements were conducted [41, 42].

3.2.2. Thermogravimetric Analysis (TGA)

Figure 7A compares the thermograms of chitin monofilaments spun at a T_C of 70 °C using a d_S of 0.6 mm with that of CH-SHR powder used as a reference. The CH-SHR sample

exhibited the characteristic thermal degradation behaviour of chitin, with an initial mass loss of 6.17% occurring below 100 °C, which was attributed to the evaporation of physically adsorbed water. This was followed by the primary polymer degradation between 300 °C and 350 °C due to deacetylation and cleavage of glycosidic bonds [43]. A final degradation stage occurred above 350 °C, associated with pyranose ring decomposition and residual carbon degradation [44].

In contrast, the chitin monofilaments displayed additional low-temperature mass losses and a shift of the main degradation steps towards lower temperatures. This indicates the presence of residual EMIMOPr and enhanced water retention, resulting from intermolecular interactions between the chitin and the IL [45]. Even after a t_C of 5 min at 70 °C, significant solvent-related mass losses were observed, demonstrating incomplete solvent removal under these conditions.

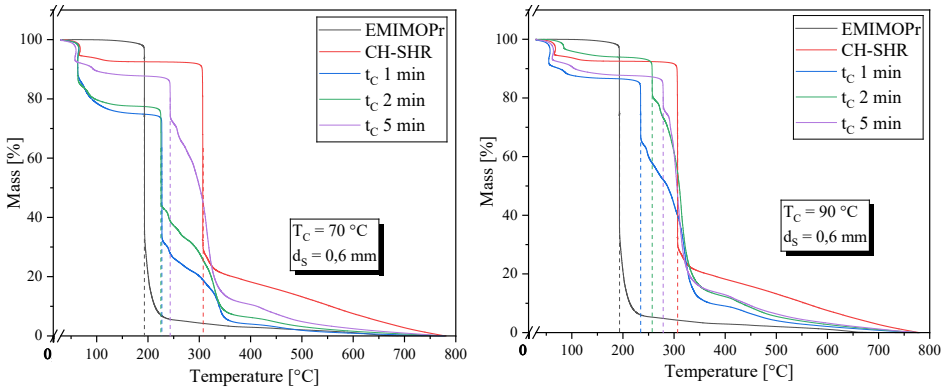

Figure 7. Thermograms of CH-SHR and chitin monofilaments (d_S = 0.6 mm) spun at (a) T_C = 70 °C and (b) T_C = 90 °C as a function of coagulation time (t_C).

Figure 7b shows the thermograms of monofilaments spun at an increased T_C of 90 °C. Although a higher T_C accelerated solvent removal, monofilaments produced at short residence times still exhibited pronounced deviations from the thermal behaviour of CH-SHR, confirming the persistence of residual solvent. As t_C increased, the onset of thermal degradation shifted progressively towards higher temperatures, approaching those of pure chitin. However, even at a t_C of 5 min and a T_C of 90 °C, complete solvent removal was not achieved.

Overall, TGA analysis revealed the presence of residual EMIMOPr within the filament core, despite processing conditions that FTIR had suggested were sufficient for solvent removal. This discrepancy highlights the limited penetration depth of FTIR spectroscopy and emphasises the need for additional, bulk-sensitive techniques to reliably detect solvents. However, it should also be noted that quantitative determination of residual solvent content by TGA is challenging, as overlapping mass-loss events from moisture, residual solvent, and polymer degradation can occur over similar temperature ranges. Consequently, the TGA results were employed to qualitatively assess solvent removal rather than to precisely quantify it.

Crucially, the observed acceleration of solvent removal with decreasing filament diameter and increasing coagulation bath temperature provides a clear mechanistic basis for process development on a larger scale. In multifilament spinning, substantially reduced individual filament diameters combined with extended residence times in the coagulation

and washing stages fundamentally alter diffusion pathways, significantly enhancing solvent removal efficiency. Therefore, the limitations observed during monofilament spinning do not represent an intrinsic barrier to producing solvent-free chitin yarns; rather, they reflect diffusion constraints that depend on scale and geometry. It should be noted that solvent removal is not solely governed by diffusion within the filament, but may also be influenced by interfacial mass transfer processes at the boundary between the filament and the coagulation medium. Consequently, the observed behaviour should be interpreted as being controlled by mass transport rather than being purely diffusion-limited.

3.3. Chitin Multifilament Yarns

3.3.1. Pilot-Scale Spinning of Chitin Multifilament Yarns

The spinning of chitin multifilament yarns was carried out under pilot-scale conditions using the wet spinning process described in Section 2.5 (Figure 8). A summary of the applied process parameters, including delivery rates, spinneret geometries, drawing ratios and take-up speeds, is provided in Table 1. It should be noted that the reported drawing ratios are below unity, indicating that slight compression of the filaments occurred along the spinning line rather than drawing. This behaviour arises from the relationship between the extrusion rate and the take-up speed, where the volumetric flow rate exceeds the final winding speed. Such processing conditions are typical of chitin- and chitosan-based wet spinning systems, in which rapid solvent/non-solvent exchange induces early phase separation and the formation of a solidified outer layer [25, 34]. This heterogeneous structure, consisting of a relatively rigid outer layer and a solvent-rich core, restricts stress distribution and molecular reorientation during drawing. Consequently, effective post-jet drawing is limited, resulting in filament breakage at relatively low deformation levels.

The EMIMOPr/CH-SHR spinning dopes were extruded through spinnerets with different geometries to evaluate process stability and filament formation. The results demonstrate that spinneret design strongly influences the robustness of the spinning process. Stable and continuous multifilament spinning was achieved using the 90 µm/300f geometry, enabling continuous filament extrusion, drawing and winding. In contrast, spinnerets with 70 µm/148f and 160 µm/24f geometries demonstrated pronounced process instability, characterised by repeated filament breakage at the spinneret and at the godet units, hindering continuous spinning. Measured yarn properties, like filament diameter, linear density and qualitative characteristics of the resulting CH-SHR-based multifilament yarns are summarised in Table 3.

The pilot-scale spinning trials prove that the wet spinning process developed using EMIMOPr can be successfully applied to both monofilament processing and continuous multifilament yarn production. However, achieving an optimal balance between spinneret geometry and filament formation conditions is crucial. Notably, stable operation was achieved with the 90 µm/300f spinneret, indicating that process robustness is influenced not only by polymer-solvent chemistry, but also by the interplay between filament count, individual filament diameter, and the mechanical stresses acting on the filament bundle during take-up.

The frequent filament breakage observed for the 70 µm/148f and 160 µm/24f geometries suggests that either insufficient filament consolidation during coagulation or unfavourable stress distribution across the filament bundle can critically limit continuous spinning. These instabilities are consistent with a diffusion-controlled solidification mechanism, in which the temporal and spatial evolution of filament strength is governed by solvent exchange and network formation. Even minor variations in local coagulation kinetics under these conditions can result in weak filament sections that break under the

tensile loads applied during exit from the spinneret and throughout the godet sequence. In addition to the geometry of the spinneret itself, the local flow conditions during filament formation are determined by the combination of delivery volume, number of capillaries and capillary diameter (Table 1). Although the total volumetric flow rate was adjusted via the gear pump, significant differences in individual filament throughput and extrusion velocity arise depending on the spinneret configuration. Specifically, a greater number of capillaries at comparable delivery rates results in lower flow per filament. In contrast, larger capillary diameters combined with fewer filaments lead to increased local extrusion velocities. These differences directly affect initial filament formation, including elongational flow, coagulation kinetics, and filament structure development.

Notably, the performance of the 90 µm/300f geometry aligns with the solvent removal behaviour-related findings obtained in monofilament spinning. Reduced filament diameters in multifilament spinning shorten transport pathways, accelerate solvent removal and promote faster filament solidification. This improves mechanical integrity during handling. The formation of homogeneous yarns with well-separated filaments suggests that the specified process parameters minimise filament bonding while enabling consistent bundle cohesion. This is a key requirement for textile processing, as it directly affects yarn uniformity, mechanical reproducibility, and subsequent handling in textile conversion steps.

Table 3. Filament diameter, linear density and qualitative characteristics of chitin multifilament yarns manufactured on a pilot scale from EMIMOPr/CH-SHR spinning dopes.

Yarn sample	Filament diameter [µm]	Linear density [tex]	Characteristics of the yarn
CH-SHR-1	37.38 ± 1.19	112.58 ± 3.91	Homogenous yarn with partially mechanically separable filaments
CH-SHR-2	29.02 ± 4.69	124.53 ± 1.06	Homogenous yarn with well-separated individual filaments
CH-SHR-3	21.08 ± 2.82	117.03 ± 0.90	Homogenous yarn with well-separated individual filaments
CH-SHR-4	45.61 ± 5.49	53.55 ± 3.42	Less homogeneous yarn with bonded filaments

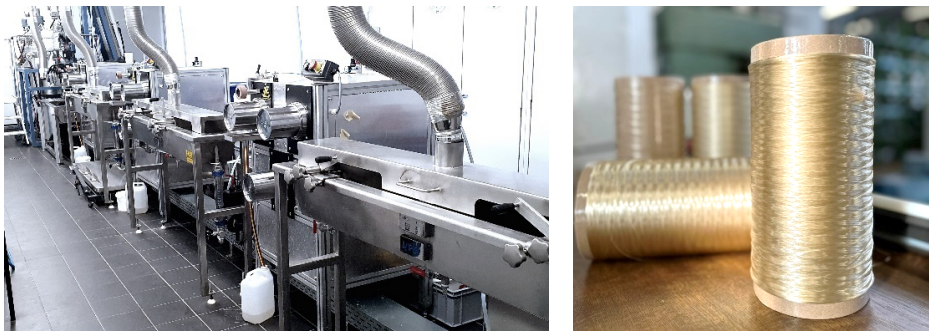

(a) **(b)**

Figure 8. (a) Pilot-Scale wet-spinning plant (Fourné Maschinenbau GmbH, Alfter-Impekoven, Germany) and (b) chitin multifilament yarn manufactured from CH-SHR/EMIMOPr spinning dopes.

3.3.2. Morphological Characterisation

SEM analysis revealed a dense, homogeneous filament structure across all multifilament yarns (Figure 9). The individual filaments exhibited closed, continuous surfaces with distinct fibrillar features, indicating uniform formation and solidification during the wet spinning process. Of the samples investigated, CH-SHR-3 demonstrated the highest morphological uniformity, characterised by smooth, defect-free filaments with a consistent diameter throughout the yarn (Figure 9b).

Cross-sectional microscopy revealed that the filaments were predominantly circular with minor deformations and shallow grooves or indentations at the contact interfaces (Figure 10). This can be attributed to local compaction within the multifilament bundle during coagulation and subsequent handling.

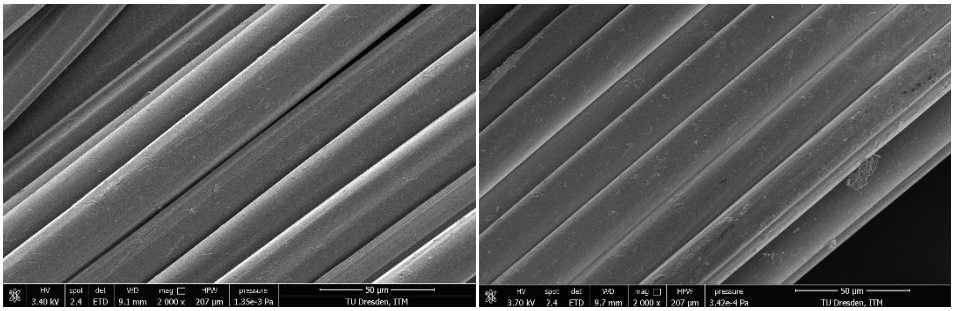

(a) **(b)**

Figure 9. SEM micrographs of chitin multifilament yarns from EMIMOPr/CH-SHR spinning dopes: (a) CH-SHR-1, (b) CH-SHR-3.

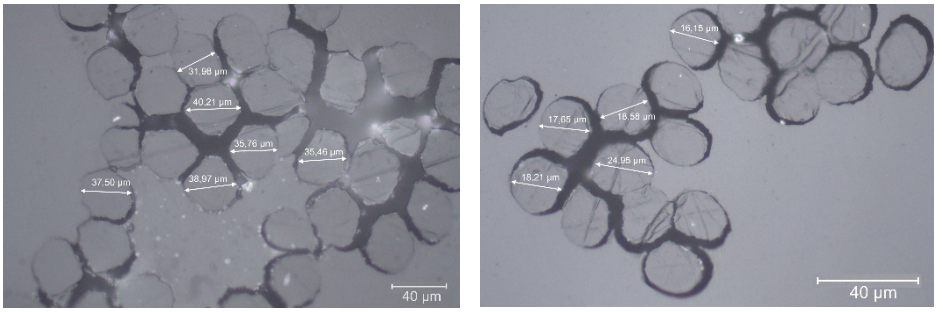

(a) **(b)**

Figure 10. Light microscopy images of filament cross sections of EMIMOPr/CH-SHR multifilament yarns (50× magnification): (a) CH-SHR-1, (b) CH-SHR-3.

3.3.3. Chemical Composition of Chitin Multifilament Yarns

FTIR spectroscopy was used to analyse the chemical composition of chitin multifilament yarns at different stages of the spinning process, in order to assess solvent removal behaviour during processing. Figure 11 compares the FTIR spectra of the raw chitin powder (CH-SHR) with those of the resulting multifilament yarns after spinning, using sample CH-SHR-3 as a representative example. No changes to the characteristic absorption bands of chitin were observed, indicating that the spinning process did not affect the chemical structure. Furthermore, no residual solvent signals were detected in the final yarns.

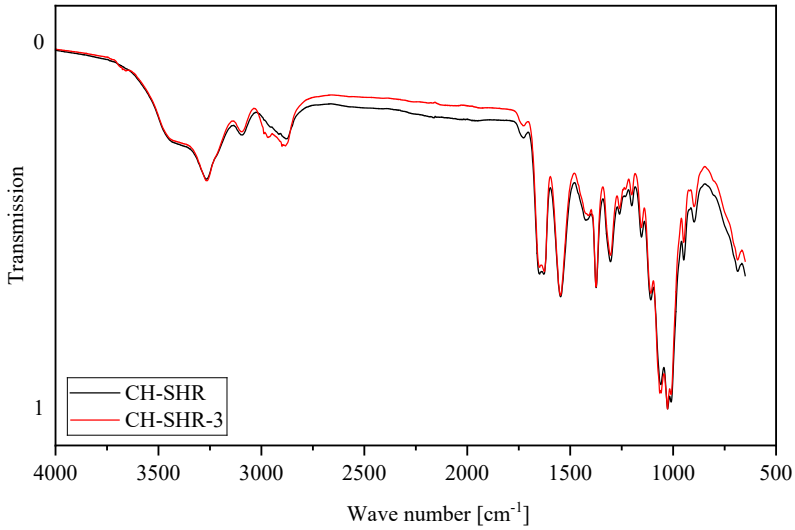

Figure 11. FTIR spectra (4000–700 cm^{-1}) of CH-SHR powder and the resulting multifilament yarns after spinning.

To analyse the removal of EMIMOPr along the entire spinning line, samples were collected after the coagulation bath (CB) and after each washing bath (WB1-WB3), then analysed using FTIR. Figure 12a shows representative spectra of CH-SHR-3 multifilament yarns, together with EMIMOPr and CH-SHR reference spectra. Solvent detection focused on the spectral region between 1700 cm^{-1} and 1425 cm^{-1}, which includes the amide I and II bands of chitin and the characteristic C=N band of EMIMOPr. The FTIR results clearly demonstrate a continuous reduction in EMIMOPr content along the coagulation and washing sequence. A comparatively high solvent content was detected immediately after the CB, which decreased progressively after each subsequent washing step. After the final washing bath (WB3), no solvent residues were detectable within the sensitivity limits of FTIR (Figure 12a).

Although FTIR analysis does not indicate any solvent residues after the washing stages, this technique is limited to near-surface regions. However, the complementary TGA results did not indicate any further mass loss related to solvents, suggesting that residual solvent within the filament core is negligible (Figure 12b). Samples collected after the CB and WB1 exhibited noticeable shifts in degradation temperature, indicating the presence of residual solvent. By contrast, samples taken after WB2 and WB3 exhibited thermal degradation behaviour comparable to that of pure CH-SHR, confirming efficient removal of the solvent. Nevertheless, it cannot be completely excluded that minor solvent amounts (below the detection limit of the applied method) are present. Consequently, it is not possible to unambiguously assign individual mass loss steps to residual IL, which limits the accuracy of determining the solvent content quantitatively. However, the combined FTIR and TGA results in this study show no detectable solvent residues within the methods' sensitivity limits, indicating that EMIMOPr can be effectively removed from the chitin multifilament yarns during continuous spinning under the developed process conditions (Table 2).

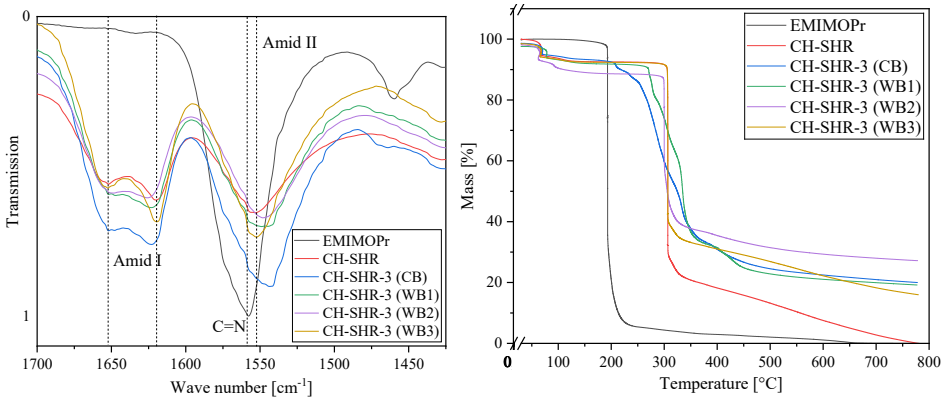

Figure 12. (a) FTIR spectra (1700–1425 cm^{-1}) of EMIMOPr, CH-SHR and resulting chitin multifilament yarns sampled after the coagulation bath (CB) and washing baths (WB1-WB3); (b) corresponding TGA thermograms (30–800 °C) at different spinning process stages.

3.3.4. Textile-Physical Properties

The textile-mechanical properties of the chitin multifilament yarns were evaluated using tensile testing in accordance with DIN EN ISO 1973. Table 4 shows the tensile strength and elongation at break of CH-SHR-based multifilament yarns at different spinneret geometries. Depending on spinneret geometry, the tensile strength of the chitin multifilament yarns ranged between ~10–20 cN/tex. The highest strengths were achieved with CH-SHR-2 and CH-SHR-3 yarns spun using a 90 µm/300f spinneret. Yarns manufactured using 70 µm/148f and 160 µm/24f spinnerets exhibited greater elongation at break (≥ 2 %), but also greater variability, due to lower draw ratios during spinning. By contrast, CH-SHR-2 and CH-SHR-3 showed elongations of around 1–2%. However, the mechanical properties of the multifilament yarns cannot be attributed solely to spinneret geometry, but must be considered in the context of the combined effects of drawing ratio, filament packing and local formation conditions. The applied drawing ratio (Table 1) determines the degree of molecular orientation and structural consolidation of the filaments. At the same time, variations in extrusion velocity between different spinneret configurations influence the effective deformation history of individual filaments prior to and during coagulation. Additionally, filament packing within the multifilament bundle considerably affects mechanical performance. Differences in filament count and diameter affect packing density and interaction between adjacent filaments. This, in turn, influences load transfer and stress distribution within the yarn. Yarns with a higher number of finer filaments (e.g. 90 µm/300f) tend to exhibit more uniform stress distribution and improved load sharing, resulting in higher tensile strength and more consistent mechanical behaviour. Conversely, systems with fewer or coarser filaments are more susceptible to localised stress concentrations and structural inhomogeneities. Furthermore, the microstructure of the filaments is affected by the interplay of solvent removal, coagulation kinetics and drawing, and this significantly impacts the final mechanical properties. Changes to these parameters can lead to variations in fibrillar structure, porosity, and internal stress distribution, making direct comparison of spinneret effects more difficult.

Knot tensile tests revealed a significant reduction in tensile strength when a knot was present (Table 4). Due to the semi-crystalline structure of chitin, which makes it more

brittle than chitosan [46], the yarns exhibited low elongation at break (≤ 3%) and pronounced knot sensitivity. This behaviour can be attributed to strong local stress concentrations and fibre bending-compression effects within the knot, which promote premature filament fracture and limit the effective load transfer within the multifilament bundle. Consequently, knot performance is a critical parameter for applications involving complex textile processing or surgical handling, and should be considered in future process optimisation strategies aimed at improving ductility and damage tolerance.

Table 4. Textile-mechanical properties of the EMIMOPr/CH-SHR multifilament yarns.

Yarn sample	Tensile strength [cN/tex]	Elongation at break [%]	Maximum tensile force [N]	Knot breaking force [N]
CH-SHR-1	15.26 ± 1.07	2.29 ± 0.53	14.43 ± 1.38	2.69 ± 0.56
CH-SHR-2	20.20 ± 1.91	2.33 ± 0.45	25.15 ± 2.38	3.01 ± 0.58
CH-SHR-3	20.27 ± 1.85	1.70 ± 0.23	25.75 ± 2.34	3.06 ± 1.25
CH-SHR-4	9.37 ± 0.97	1.33 ± 0.29	10.54 ± 1.09	1.88 ± 1.10

The large-scale production and commercial availability of pure chitin or chitosan fibres are currently very limited [47], which makes direct comparison with established industrial materials challenging. However, Li *et al.* [48] recently reported tensile strengths of up to 19 cN/tex with filament diameters in the range of 10–15 µm for commercially available chitosan fibres (e.g. Jifa Group Co., Dongyang, PRC). These values are comparable to those obtained in the present study, where tensile strengths of up to approximately 20 cN/tex were achieved. However, the referenced study does not provide any detailed information on processing conditions, solvent systems, polymer purity or fibre structure, which limits a direct assessment of material quality and comparability. In particular, the absence of information on solvent systems and post-processing makes it difficult to evaluate the sustainability and reproducibility of the reported fibres. Compared with established regenerated cellulose fibres such as viscose or lyocell, which typically exhibit tensile strengths of approximately 20–40 cN/tex, the chitin-based multifilament yarns produced in this study demonstrate comparable strength while retaining the intrinsic advantages of chitin, such as biodegradability and bioactivity. Considering the early stage of process development and the absence of extensive post-drawing or finishing steps, the achieved mechanical properties are promising.

Overall, the results indicate that the wet spinning of chitin using IL can produce fibres with competitive mechanical properties, providing a solid foundation for further optimisation to reach industrially relevant performance levels.

4. Conclusions

This study demonstrates the successful development and pilot-scale implementation of a solvent-based wet spinning process to manufacture chitin multifilament yarns using the ionic liquid (IL) EMIMOPr as the solvent. A systematic investigation of solvent removal behaviour revealed that mass transport processes within the filament play a key role, being strongly influenced by filament diameter, coagulation temperature, and residence time. Under laboratory-scale conditions, residual solvent can remain in the filament core, demonstrating the limitations of solvent removal in single-filament systems.

Transferring these insights to pilot-scale multifilament spinning enabled significantly improved solvent removal by reducing filament diameters and extending residence times in the coagulation and washing stages. FTIR and TGA analyses indicated the effective removal of EMIMOPr within the detection limits of the applied methods, with no evidence of the chemical modification of chitin. The resulting yarns exhibited homogeneous morphology and consistent textile-mechanical properties. However, the quantitative determination of residual solvent content remains challenging due to overlapping thermal degradation processes and cannot be resolved unambiguously using TGA and FTIR alone. A more detailed quantitative analysis requires additional calibration or complementary analytical methods in the future.

Overall, these results demonstrate a robust, scalable processing approach for chitin filament yarns using ILs, providing a solid platform for further industrial implementation in the biomedical and textile industries.

5. Acknowledgements and Funding

The IGF research project 22568 BR/1 of the Forschungsvereinigung Forschungskuratorium Textil e. V. was funded by the AiF within the program for supporting the "Industrielle Gemeinschaftsforschung (IGF)" from funds of the German Federal Ministry for Economic Affairs and Climate Action (BMWE) on the basis of a decision by the German Bundestag. The authors wish to thank BMWE for financial support. The authors gratefully acknowledge proionic GmbH for providing the ionic liquid used in this study.

6. Author Contributions

Conceptualisation, I.K. and C.K.; methodology, I.K. and C.K.; validation, I.K. and C.K.; formal analysis, I.K. and C.K.; investigation, I.K., C.K., S.S., and E.S.; writing—original draft preparation, I.K. and C.K.; writing—review and editing, L.B. and C.C.; project administration, C.C. All authors have read and agreed to the published version of the manuscript. I.K. and C.K. are considered joint first authors, as they contributed equally to this work.

7. References

[1] Aibibu D, Hild M, Wöltje M, Cherif C; (2016) Textile cell-free scaffolds for in situ tissue engineering applications. Journal of Materials Science: Materials in Medicine 27(3), 63. **DOI:** 10.1007/s10856-015-5656-3

[2] Wu Y, Han Y, Wong YS, Fuh JYH; (2018) Fibre-based scaffolding techniques for tendon tissue engineering. Journal of Tissue Engineering and Regenerative Medicine 12(7), 1798–1821. **DOI:** 10.1002/term.2701

[3] Dong L, Wichers HJ, Govers C; (2019) Beneficial health effects of chitin and chitosan. In: Broek LAM, Boeriu CG (eds.), Chitin and Chitosan, 1st ed., Wiley, Hoboken, NJ, Chichester, pp. 145–167. **DOI:** 10.1002/9781119450467.ch6

[4] Singh R, Shitiz K, Singh A; (2017) Chitin and chitosan: biopolymers for wound management. International Wound Journal 14(6), 1276–1289. **DOI:** 10.1111/iwj.12797

[5] Chang C, Peng N, He M, Teramoto Y, Nishio Y, Zhang L; (2013) Fabrication and properties of chitin/hydroxyapatite hybrid hydrogels as scaffold nano-materials. Carbohydrate Polymers 91(1), 7–13. **DOI:** 10.1016/j.carbpol.2012.07.070

[6] He M *et al.*; (2017) Biocompatible and biodegradable bioplastics constructed from chitin via a "green" pathway for bone repair. ACS Sustainable Chemistry & Engineering 5(10), 9126–9135. **DOI:** 10.1021/acssuschemeng.7b02051

[7] Maeda Y, Jayakumar R, Nagahama H, Furuike T, Tamura H; (2008) Synthesis, characterization and bioactivity studies of novel β-chitin scaffolds for tissue-engineering applications. International Journal of Biological Macromolecules 42(5), 463–467. **DOI:** 10.1016/j.ijbiomac.2008.03.002

[8] Wan ACA, Tai BCU; (2013) CHITIN — A promising biomaterial for tissue engineering and stem cell technologies. Biotechnology Advances 31(8), 1776–1785. **DOI:** 10.1016/j.biotechadv.2013.09.007

[9] Shamshina JL; (2019) Chitin in ionic liquids: historical insights into the polymer's dissolution and isolation. A review. Green Chemistry 21(15), 3974–3993. **DOI:** 10.1039/C9GC01830A

[10] Aworinde AK, Taiwo OO, Adeosun SO, Akinlabi ET, Jonathan H, Olayemi OA, Joseph OO; (2021) Biodegradation profiles of chitin, chitosan and titanium reinforced polylactide biocomposites as scaffolds in bone tissue engineering. Arab Journal of Basic and Applied Sciences 28(1), 351–359. **DOI:** 10.1080/25765299.2021.1971865

[11] Levengood SKL, Zhang M; (2014) Chitosan-based scaffolds for bone tissue engineering. Journal of Materials Chemistry B 2(21), 3161. **DOI:** 10.1039/c4tb00027g

[12] Shamshina JL, Berton P, Rogers RD; (2019) Advances in functional chitin materials: a review. ACS Sustainable Chemistry & Engineering 7(7), 6444–6457. **DOI:** 10.1021/acssuschemeng.8b06372

[13] Tao F, Cheng Y, Shi X, Zheng H, Du Y, Xiang W, Deng H; (2020) Applications of chitin and chitosan nanofibers in bone regenerative engineering. Carbohydrate Polymers 230, 115658. **DOI:** 10.1016/j.carbpol.2019.115658

[14] Venkatesan J, Kim S-K; (2010) Chitosan composites for bone tissue engineering—an overview. Marine Drugs 8(8), 2252–2266. **DOI:** 10.3390/md8082252

[15] Roy JC, Salaün F, Giraud S, Ferri A, Chen G, Guan J; (2017) Solubility of chitin: solvents, solution behaviors and their related mechanisms. In: Xu Z (ed.), Solubility of Polysaccharides, InTechOpen. **DOI:** 10.5772/intechopen.71385

[16] Chitin fibers and process for the production of the same. **Patent** US4932404A; (1990) Kifune K, Inoue K, Mori S. United States.

[17] Tokura S, Nishi N, Noguchi J; (1979) Studies on chitin. III. Preparation of chitin fibers. Polymer Journal 11(10), 781–786. **DOI:** 10.1295/polymj.11.781

[18] Tokura S, Yoshida J, Nishi N, Hiraoki T; (1982) Studies on chitin. VI. Preparation and properties of alkyl-chitin fibers. Polymer Journal 14(7), 527–536. **DOI:** 10.1295/polymj.14.527

[19] Mikhailov GM, Lebedeva MF, Nud'ga LA, Petrova VA; (2001) Composite fibers based on chitin and cellulose. Russian Journal of Applied Chemistry 74(9), 1573–1576. **DOI:** 10.1023/A:1013734008473

[20] Nguyen KD; (2021) Temperature effect of water coagulation bath on chitin fiber prepared through wet-spinning process. Polymers 13(12), 1909. **DOI:** 10.3390/polym13121909

[21] Pillai CKS, Paul W, Sharma CP; (2009) Chitin and chitosan polymers: Chemistry, solubility and fiber formation. Progress in Polymer Science 34(7), 641–678. **DOI:** 10.1016/j.progpolymsci.2009.04.001

[22] Matthews BD, Paton L; (2018) Updates in mesh and biomaterials. Surgical Clinics of North America 98(3), 463–470. **DOI:** 10.1016/j.suc.2018.02.007

[23] Butler CE, Baumann DP, Janis JE, Rosen MJ; (2013) Abdominal wall reconstruction. Current Problems in Surgery 50(12), 557–586. **DOI:** 10.1067/j.cpsurg.2013.08.003

[24] Ota A, Beyer R, Hageroth U, Müller A, Tomasic P, Hermanutz F, Buchmeiser MR; (2021) Chitin/cellulose blend fibers prepared by wet and DRY-WET spinning. Polymers for Advanced Technologies 32(1), 335–342. **DOI:** 10.1002/pat.5089

[25] Kuznik I, Kruppke I, Pötzsch HF, Cherif C; (2024) Pure chitosan multifilament yarns made using a semi-industrial pilot scale wet-spinning process with ionic liquids. Journal of Applied Polymer Science 141(23), e55457. **DOI:** 10.1002/app.55457

[26] Mundsinger K, Müller A, Beyer R, Hermanutz F, Buchmeiser MR; (2015) Multifilament cellulose/chitin blend yarn spun from ionic liquids. Carbohydrate Polymers 131, 34–40. **DOI:** 10.1016/j.carbpol.2015.05.065

[27] Shamshina JL, Zavgorodnya O, Berton P, Chhotaray PK, Choudhary H, Rogers RD; (2018) Ionic liquid platform for spinning composite chitin–poly(lactic acid) fibers. ACS Sustainable Chemistry & Engineering 6(8), 10241–10251. **DOI:** 10.1021/acssuschemeng.8b01554

[28] Kuznik I, Kruppke I, Cherif C; (2022) Pure chitosan-based fibers manufactured by a wet spinning lab-scale process using ionic liquids. Polymers 14(3), 477. **DOI:** 10.3390/polym14030477

[29] Schröder T; (2020) Rheologie der Kunststoffe: Theorie und Praxis. Carl Hanser Verlag GmbH & Co. KG, München, Germany. **DOI:** 10.1007/978-3-446-46550-3

[30] Hermanutz F, Vocht MP, Panzier N, Buchmeiser MR; (2019) Processing of cellulose using ionic liquids. Macromolecular Materials and Engineering 304(2), 1800450. **DOI:** 10.1002/mame.201800450

[31] Walther P, Ota A, Müller A, Hermanutz F, Gähr F, Buchmeiser MR; (2016) Chitin foils and coatings prepared from ionic liquids. Macromolecular Materials and Engineering 301(11), 1337–1344. **DOI:** 10.1002/mame.201600208

[32] Ng PF, Lee KI, Meng S, Zhang J, Wang Y, Fei B; (2019) Wet spinning of silk fibroin-based core–sheath fibers. ACS Biomaterials Science & Engineering 5(6), 3119–3130. **DOI:** 10.1021/acsbiomaterials.9b00275

[33] Karkhanechi H, Vaselbehagh M, Jeon S, Shaikh AR, Wang D, Matsuyama H; (2018) Preparation and characterization of polyvinylidenedifluoride-co-chlorotrifluoroethylene hollow fiber membranes with high alkaline resistance. Polymer 145, 310–323. **DOI:** 10.1016/j.polymer.2018.04.074

[34] Toskas G, Brünler R, Hund H, Hund R-D, Hild M, Aibibu D, Cherif C; (2013) Pure chitosan microfibres for biomedical applications. Autex Research Journal 13(4), 134–140. **DOI:** 10.2478/v10304-012-0041-5

[35] Ren F, Wang J, Yu J, Zhong C, Xie F, Wang S; (2022) Green synthesis of acetylated maize starch in different imidazolium carboxylate and choline carboxylate ionic liquids. Carbohydrate Polymers 288, 119353. **DOI:** 10.1016/j.carbpol.2022.119353

[36] Zhao B, Greiner L, Leitner W; (2012) Cellulose solubilities in carboxylate-based ionic liquids. RSC Advances 2(6), 2476. **DOI:** 10.1039/c2ra01224c

[37] Chen X, Chew SL, Kerton FM, Yan N; (2014) Direct conversion of chitin into a N-containing furan derivative. Green Chem 16(4), 2204–2212. **DOI:** 10.1039/C3GC42436G

[38] Kaya M, Erdogan S, Mol A, Baran T; (2015) Comparison of chitin structures isolated from seven Orthoptera species. International Journal of Biological Macromolecules 72, 797–805. **DOI:** 10.1016/j.ijbiomac.2014.09.034

[39] Um IC, Kweon H, Lee KG, Ihm DW, Lee J-H, Park YH; (2004) Wet spinning of silk polymer. International Journal of Biological Macromolecules 34(1–2), 89–105. **DOI:** 10.1016/j.ijbiomac.2004.03.007

[40] Kaur H, Rana B, Tomar D, Kaur S, Jena KC; (2021) Fundamentals of ATR-FTIR spectroscopy and its role for probing in-situ molecular-level interactions. In: Singh DK, Pradhan M, Materny A (eds.), Modern Techniques of Spectroscopy, Vol. 13, Springer Singapore, Singapore, pp. 3–37. **DOI:** 10.1007/978-981-33-6084-6_1

[41] Neville GA, Beckstead HD, Cooney JD; (1994) Thermal analyses (TGA and DSC) of some spironolactone solvates. Fresenius' Journal of Analytical Chemistry 349(10–11), 746–750. **DOI:** 10.1007/BF00325651

[42] Wei Y, Jang G-W, Hsueh KF, Scherr EM, MacDiarmid AG, Epstein AJ; (1992) Thermal transitions and mechanical properties of films of chemically prepared polyaniline. Polymer 33(2), 314–322. **DOI:** 10.1016/0032-3861(92)90988-9

[43] Ziegler-Borowska M, Chełminiak D, Kaczmarek H; (2015) Thermal stability of magnetic nanoparticles coated by blends of modified chitosan and poly(quaternary ammonium) salt. Journal of Thermal Analysis and Calorimetry 119(1), 499–506. **DOI:** 10.1007/s10973-014-4122-7

[44] Moussout H, Ahlafi H, Aazza M, Bourakhouadar M; (2016) Kinetics and mechanism of the thermal degradation of biopolymers chitin and chitosan using thermogravimetric analysis. Polymer Degradation and Stability 130, 1–9. **DOI:** 10.1016/j.polymdegradstab.2016.05.016

[45] Xiong Y, Wang H, Wu C, Wang R; (2012) Preparation and characterization of conductive chitosan–ionic liquid composite membranes. Polymers for Advanced Technologies 23(11), 1429–1434. **DOI:** 10.1002/pat.2061

[46] Teng S, Lee E, Yoon B, Shin D, Kim H, Oh J; (2009) Chitosan/nanohydroxyapatite composite membranes via dynamic filtration for guided bone regeneration. Journal of Biomedical Materials Research Part A 88A(3), 569–580. **DOI:** 10.1002/jbm.a.31897

[47] Veit D; (2023) Fasern: Geschichte, Erzeugung, Eigenschaften, Markt. Springer Berlin Heidelberg, Berlin, Heidelberg. **DOI:** 10.1007/978-3-662-64469-0

[48] Li J, Fu J, Tian X, Hua T, Poon T, Koo M, Chan W; (2022) Characteristics of chitosan fiber and their effects towards improvement of antibacterial activity. Carbohydrate Polymers 280, 119031. **DOI:** 10.1016/j.carbpol.2021.119031

© Polish Chitin Society

Open Access: This article is distributed under the terms of the Creative Commons Attribution 4.0 International License (CC BY 4.0), which permits use, sharing, adaptation, distribution and reproduction in any medium or format, provided that appropriate credit is given to the original author(s) and source, a link to the license is provided, and any changes are indicated. Third-party material is included under the same license unless otherwise stated in a credit line.